Towards Event-Based Satellite Docking: A Photometrically Accurate Low-Earth Orbit Hardware Simulation

Nuwan Munasinghe[1], Cedric Le Gentil[1], Jack Naylor[2], Mikhail Asavkin[3],
Donald G. Dansereau[2], Teresa Vidal-Calleja[1]

Abstract— Automated satellite docking is a prerequisite for most future in-orbit servicing missions. Most vision-based solutions proposed use conventional cameras. However, conventional cameras face challenges due to extreme illumination conditions. Event cameras have been used in various applications because of their advantages over conventional cameras, such as high temporal resolution, higher dynamic range, low power consumption, and higher pixel bandwidth. This paper presents a hardware setup to simulate low earth orbit (LEO) conditions. The setup aims to show the suitability of event-based cameras for satellite docking applications. The developed test environment has lighting conditions similar to LEO, a mock-up satellite's docking port following Lockheed Martin's Mission Augmentation Port standard, and a robotic arm that can move the mock-up satellite to replicate movements in space. This paper shows the drawbacks faced by traditional cameras in LEO conditions, such as pixel saturation, resulting in feature loss. To overcome these limitations, this paper presents a port detection pipeline using event-based cameras. The proposed pipeline detects the docking port with an average error of 8.58 pixels in image space. This error compared to the image width and height is 2.48% and 3.30% respectively. Therefore, the proposed method provides promising results towards satellite docking using event cameras in the LEO environment where illumination conditions are challenging.

I. INTRODUCTION

Satellite docking is a key component for in-orbit servicing missions like refuelling, diagnostics, de-orbiting or component replacement. To dock to a satellite in space, one spacecraft must match the orbital parameters of another and successfully rendezvous. Our research is currently focused on detecting and tracking a docking port to develop a navigation and control system for satellite docking. In space, standard cameras are limited by illumination conditions, ranging from intense direct illumination to full shadow. We discuss the suitability of event cameras [1] for satellite docking under these conditions, leveraging the high dynamic range of event sensors.

Moreover, this work presents the hardware simulation environment developed to simulate low earth orbit (LEO) illumination conditions over a mock-up satellite's docking port following Lockheed Martin's Mission Augmentation Port standard [2]. Fig. 1 shows an image of the proposed hardware test-bench. Given this LEO simulated setup, we show the use of event-based camera data to overcome the
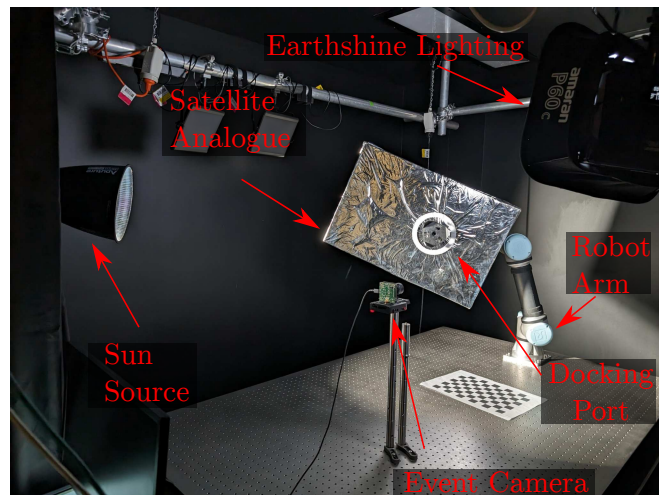
Fig. 1. LEO test bench demonstrating the location of key hardware. Our satellite analogue is mounted to the end of a UR5e robotic arm in front of a DAVIS 346 event camera. We use an Aputure LS1200D to simulate sunlight, and three Aputure P60c panel lights with diffusers to simulate Earthshine.

limitations of standard cameras. We propose a pipeline that processes accumulated event data to detect the centre of the docking port in an image generated from events. The proposed system is a step towards semi-autonomous docking using event cameras. This system will leverage the advantages of event cameras including minimal motion blur, low latency, low power consumption and high dynamic range imaging [3] within the orbital environment.

II. LITERATURE REVIEW

Compared to standard cameras that capture images at a fixed frame rate, event cameras measure changes to individual pixel brightness asynchronously and provide a stream of events that include time, location and sign of the brightness change [4]. Event cameras have properties like high temporal resolution, high dynamic range, low power consumption, and high pixel bandwidth [4]. Therefore, event cameras have a high potential in robotics and vision scenarios that are challenging for standard cameras, such as high-speed, low-latency and higher dynamic range [4]. Applications of event cameras include object tracking [5], gesture recognition [6], stereo vision [7], simultaneous localisation and mapping (SLAM) [8] and optical flow [9].

Event cameras have previously been used in space-related

applications. Samya et al. [10] used event cameras to track stars, making tracking more energy-efficient and faster. Event cameras have also been used in space situational awareness (SSA), which detects and tracks objects in orbit around the earth [3]. In SSA, using event cameras provides a high dynamic range, high-speed and low-power sensor [11]. Moshi et al. [12] used event cameras for close proximity satellite pose detection and demonstrated that event cameras provide a promising solution to generalise from the simulation to the target domain under extreme illumination changes.

Illumination conditions in space are challenging mainly because of the sunlight exposure and reflective surfaces of a satellite, which creates reflections, saturation, and missing detection. This is coupled with deep shadows associated with a lack of ambient illumination. Nassir et al. [13] used standard cameras, edge-based tracking and model matching for vision-based localisation for in-orbit servicing. With detection and tracking methods, they used a monocular camera for mid-range tracking $5\,\text{m}$ to $20\,\text{m}$ and a stereo camera at close-range $0.5\,\text{m}$ to $5\,\text{m}$. This testing was carried out in the European Proximity Operations Simulator (EPOS), a ground simulation able to create sunlight conditions using high-power floodlights, satellite appearance using multi-layer insulation sheets, as well as orbital motion trajectories [13].

LiDAR and thermal camera-based approaches have been used for autonomous docking applications [14]. This system was tested on the space shuttle Discovery during the STS-128 mission to the International Space Station. Geometric data captured by point clouds has been used to match against the previously known shape of the target object to compute its position and orientation [14]. The main advantage of this system is that it is lighting immune and has the capability to automatically rendezvous and dock [14]. Neptec's Laser Camera System-LCS [15] is another LiDAR-based system. However, their higher weight and power consumption are some of the drawbacks of using LiDAR [13].

III. TEST BENCH FOR SATELLITE DOCKING

A. Test bench setup

The setup of the test bench is shown in Fig. 1. The setup contains an Aputure LS1200D light capable of producing illumination consistent with sunlight in low earth orbit (LEO). The walls of the lab are black to reduce stray-light reflection. A satellite mock-up which includes a scaled-down docking port is mounted on a UR5e robot. This analogue of a satellite body has been constructed with Mylar to emulate multi-layered insulation (MLI) with creases and texture to match what would be seen in orbit. The mylar is secured with an epoxy backing, ensuring the texture is repeatable between trials. The mylar exhibits surface reflectivity similar to a real satellite, allowing for extreme specular reflections to be captured by the event camera. The robot arm enables repeatability of the same trajectory under different illumination conditions, allowing for pixel level comparisons between trials. A DAVIS 346 [16] is mounted onto the optical table for our experiments, however, we note that our approach generalises to other event camera types, including those
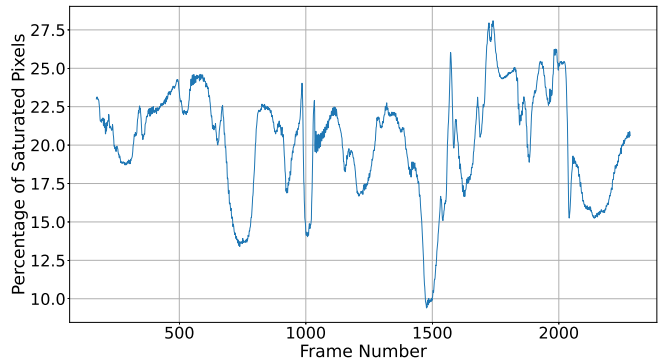

Fig. 2. Percentage of saturated pixels in RGB frames.

that do not capture intensity frames. This model of event camera provides both RGB as well as event data, enabling comparison under the same test conditions in RGB and event space through the same optical aperture. Camera intrinsic calibration was performed using the RGB image frames and checkerboard method. The extrinsic transformation between the camera and the arm's end effector is obtained by performing the hand-eye calibration with a checkerboard and the known kinematics of the UR5e. The final ground truth of the port pose in the camera's reference frame leverages the known CAD model of the satellite mock-up mounted to the end of the robot arm, along with base-to-end-effector transformations.

Orbital lighting conditions are extremely challenging because of the directional sunlight resulting in shadows and high specularities [17]. Earth's albedo also provides a source of diffuse light that can help fill shadows [14]. To replicate the directional illumination conditions, we position the Aputure LS1200D at a distance of $1.8\,\text{m}$ from the work area to produce $130\,\text{klm}\,\text{m}^{-2}$, the intensity of light at a $400\,\text{km}$ orbit. The parabolic reflector around the light produces a beam which has minimal divergence, allowing for deep shadowing to be simulated in the working area. We also utilise three Aputure P60C panel lights to produce a diffuse, blue-tinted $8178\,\text{lm}\,\text{m}^{-2}$ source to simulate Earthshine, light reflected from the surface of the Earth. Spacecraft performing orbital inspection may have lighting fitted on-board to assist with illumination when behind the Earth, and so we optionally add in a small colocated Aputure MC panel light source to simulate a spacecraft-mounted light.

B. Motivation towards event cameras

Event cameras can handle extreme illumination conditions that inhibit RGB cameras. This occurs in docking scenarios due to the high-intensity reflection of sunlight from the satellite surface and causes saturation of RGB camera pixels in all three channels. An experiment was conducted using the sunlight source and moving the satellite analogue using the robot arm in front of the camera. Fig. 2 shows the percentage of saturated pixels over time in the RGB image during this experiment. The pixel saturation depends on the relative
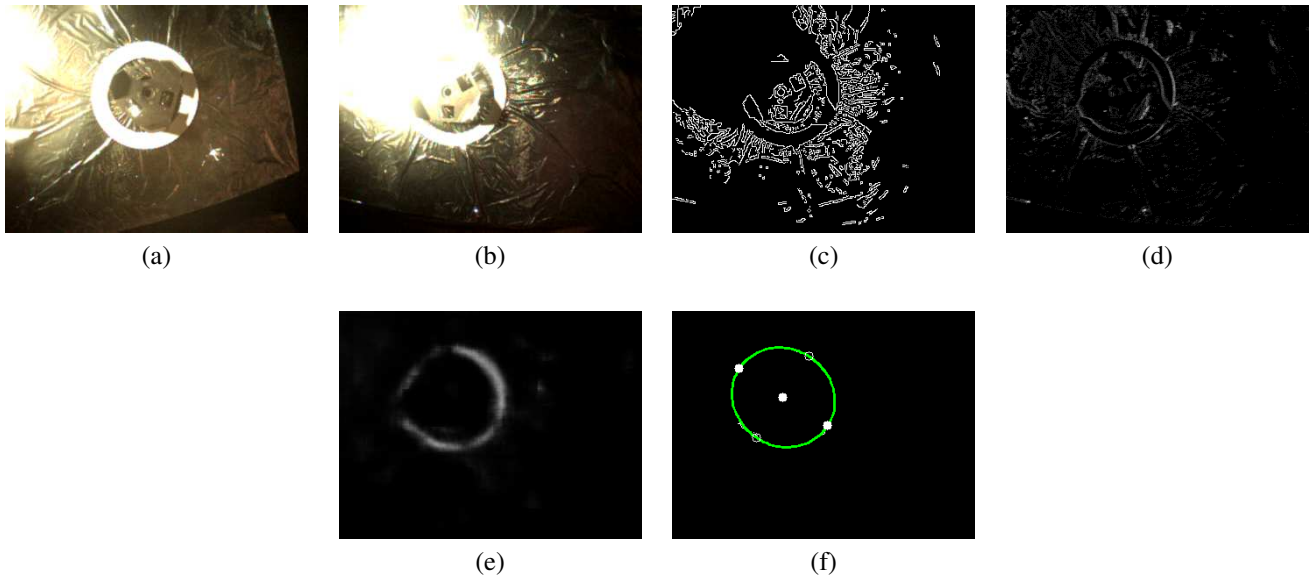
Fig. 3. (a) RGB image with less saturation around the ring region. (b) RGB image with significant saturation around the ring region. (c) Edge detection on saturated RGB image. (d) Image generated from events (accumulation of 20k events). (e) Result of filtered ring. (f) Result of fitting RANSAC ellipse (Filled white circles: ends of the major axis and centre. White empty circles: ends of the minor axis).

orientation of the light source, camera and satellite body. For example, Fig. 3(a) shows the RGB image when there is less saturation near the docking port. However, Fig. 3(b) shows how saturation occurs with reflections. In these saturated situations, it is difficult to detect reliable image features like edges near the docking port (ring), as shown in Fig. 3(c). In tracking, and downstream close-proximity operations this can cause significant issues. However, as shown by accumulating 20,000 events in Fig. 3(d), the event data show the features of the ring more clearly. This ability of the event camera to identify features in saturated illumination conditions provides strong motivation for their use in these situations.

IV. DOCKING PORT DETECTION

The Lockheed Martin Mission Augmentation Port (MAP) Standard is an open-source mechanical interface for satellites to dock in orbit [2]. In this work, we use a docking port modelled on this standard. According to the MAP standard, there are six stages of docking; approach, host system preparation for docking, soft capture, hard dock, connection testing and hand off to host [2]. This work aims to detect the docking port during the approach stage so that the orientation and trajectory of the satellite can be determined to dock successfully. The outer part of the docking port consists of a reflective circular navigational aid. In this paper, the detection of this ring is considered to determine the preliminary orientation of the satellite.

A. Docking port detection pipeline

The aforementioned navigational aid is a reflective planar ring circling the docking port. This work leverages a light source collocated with the camera to ensure the maximum visibility of the ring. Using the standard camera pin-hole model, the ring projection on the image plane is close to being an ellipse. Accordingly, the proposed method aims to estimate the ring pose in the image using the implicit representation of a conic section

$$Ax^2 + Bxy + Cy^2 + Dx + Ey + F = 0, \qquad (1)$$

with x and y a point in the image plane, and A-F the ellipse parameters. As illustrated in Fig. 4, the proposed method consists of three steps:

- Accumulation of event data into image-like histograms,
- Data-driven image filtering with a Convolutional Neural Network (CNN),
- Ellipse parameter estimate with RANSAC-based fitting.

The first step simply consists of populating a histogram with each bin corresponding to a pixel in the image plane and counting the events occurring in each cell regardless of their polarity. Such an image-like histogram is constructed for every set of N consecutive events. Unfortunately, due to the high level of texture and shadows, it is highly challenging to directly estimate the ellipse parameters. The rest of this subsection presents the proposed filtering and ellipse fitting algorithms.

1) Filter learning and training process: With the goal of satellite-agnostic port detection, the proposed method leverages a *U-Net*-like [19] CNN to learn and infer an image containing only a single ellipse at the location of the ring projection. It consists of 3 consecutive convolution layers with ReLU activation functions and max-pooling, followed by three consecutive deconvolution layers with ReLU activation. The output is an image $\mathcal{I}$, of the same size as the input histogram, that is passed through a sigmoid function to highly the ellipse with ones and setting to zero the rest of the pixels. The absence of fully connected layers forces the filter to only consider local information, thus preventing the network from overfitting by learning the position of
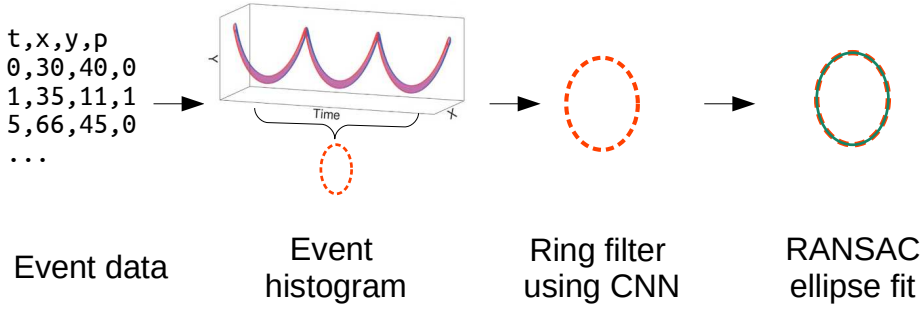
Fig. 4. Detection pipeline starting from event data to fitting an ellipse (Image source in event histogram: Kaichao You [18]).

Fig. 5. Example of textures used for physical data augmentation for training. Multiple panels have been created to be affixed around the mock-up satellite's docking port or to fully replace the mock-up.

the docking port on the specific mock-up model used for training.

The training is performed using around 20 minutes of data with a consumer-grade laptop[1]. The training data includes examples with and without the docking port. It includes "physically-augmented" sequences where various textures (other than Mylar as shown in Fig. 5) have been affixed to the mock-up satellite. The training labels are generated by drawing an ellipse with a thickness of 3 pixels at the known location of the ring's projection in the image plane using the CAD model, the known pose of the arm, and the extrinsic calibration parameters.

2) Ellipse fitting: The image-like output of the aforementioned ellipse filter $\mathcal{I}$ is binarised according to an arbitrary threshold. Then a skeletonisation step [20] is performed to obtain a one-pixel-wide representation of the scene $\mathcal{I}_S$. If no ring is present in the scene, very few pixels are "ON"/active in the skeletonised image. Accordingly, the ellipse fitting process is aborted when the number of active pixels is under a threshold γ_S. Given enough points in the skeletonised image, the active pixels are converted into a 2D point cloud $\mathbf{X}$ based on their location in the image. Then RANSAC-based ellipse fitting is performed: First, selecting randomly 5 points $\mathbf{X}_h$, the hypothesis ellipse parameters

---

[1]Training performed in less than an hour with an Nvidia RTX A500 (mobile) GPU.

Algorithm 1 RANSAC-based ellipse detection/fitting

Input: Filtered-image $\mathcal{I}$, thresholds γ_F, γ_S, γ_I, and γ_A
Output: Ellipse detection flag e, ellipse parameters $\mathbf{p}$

$\mathcal{I}_B \leftarrow \text{binarise}(\mathcal{I}, \gamma_F)$ ▷ Binarise image
$\mathcal{I}_S \leftarrow \text{skeletonise}(\mathcal{I}_B)$ ▷ Skeletonise image

$e \leftarrow False$
$n \leftarrow 0$
if $|\mathcal{I}_S| > \gamma_S$ **then** ▷ If enough active pixels
    $\mathbf{X} \leftarrow \text{coordinates}(\mathcal{I}_S)$
    for $i = (0, \cdots, N)$ **do** ▷ RANSAC fitting
        $\mathbf{X}_h \leftarrow \text{randomSelect}(\mathbf{X})$ ▷ Select 5 points
        $\mathbf{p}_h \leftarrow \text{ellipseParam}(\mathbf{X}_h)$ ▷ Hypothesis param.
        if $\text{axisRatio}(\mathbf{p}_i) > \gamma_A$ **then** ▷ Check axis ratio
            $\mathbf{X}_I \leftarrow \text{getInliers}(\mathbf{X}, \mathbf{p}_h)$
            if $|\mathbf{X}_I| > \gamma_I$ and $|\mathbf{X}_I| > n$ **then** ▷ If enough inliers
                $\mathbf{p}_h = \text{ellipseParam}(\mathbf{X}_I)$
                $e \leftarrow True$
                $\mathbf{p} \leftarrow \mathbf{p}_h$ ▷ Accept hypothesis
                $n \leftarrow |\mathbf{X}_I|$
            end if
        end if
    end for
end if
return e, $\mathbf{p}$

$\mathbf{p}_h$ are estimated by solving a linear system of equations. To comply with the difference in the number of degrees of freedom between an ellipse and the conic representation (5 vs. 6), the value of F is set to 1. The number of inliers for the current hypothesis is computed using $\mathbf{p}_h$ and all the points in $\mathbf{X}$ if the ratio between the minor over the major axis of the estimated ellipse is close enough to one (i.e., $> \gamma_A$). Otherwise, the hypothesis is disregarded. For successful hypotheses, the ellipse parameters are fitted to the set of inliers if there are enough of them. This RANSAC process is repeated N times or until the number of inliers reaches the number of points in $\mathbf{X}$. The overall process is illustrated formally in Algorithm 1.

The knowledge of the ellipse parameters enables subsequent estimation steps such as tracking or 6DoF pose estimation of the docking port in the camera frame. These tasks will be part of our future work toward autonomous satellite docking.
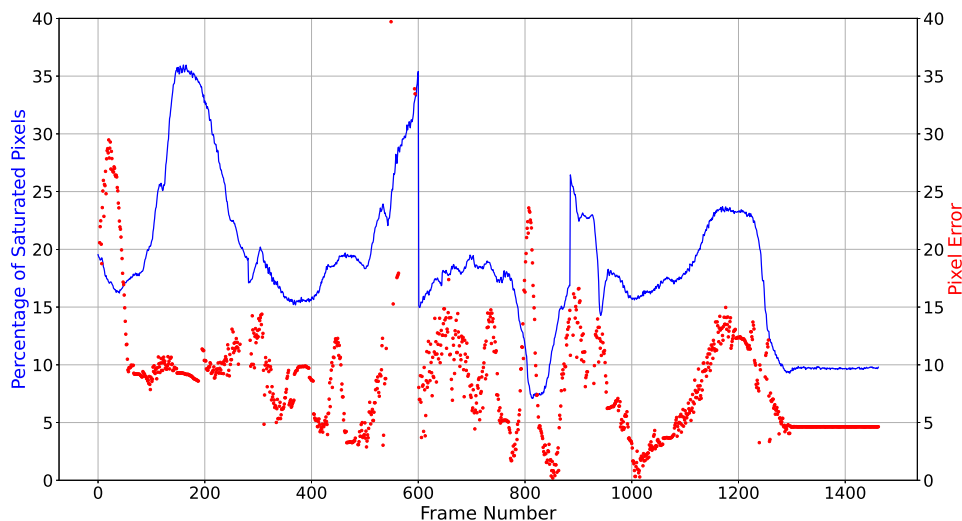
Fig. 6. Percentage of saturated pixels, Pixel Error in RoI vs Frame Number (Image size: 346 x 260 pixels).

B. Experimental results

Fig. 6 shows the experimental results of the detection pipeline. The red colour plot shows the pixel error (Euclidean distance error in 2D) between the actual ring centre (computed using the known arm position, the extrinsic calibration parameters, and the known CAD) and the predicted ring centre using the proposed pipeline. Cases where the ellipse cannot be detected due to partial ring filtering are not plotted. The blue plot shows the percentage of saturated pixels in the region of interest (RoI). The RoI is the area of the image that corresponds to the satellite mock-up (eg., in Fig. 3(a), the RoI contains the full image minus the two black triangles on the right and bottom-right).

According to these experimental results, when ellipse detection was possible using event data, the average pixel error was 8.58, and the maximum error recorded was around 39 pixels. The size of the image frame is 346 by 260. The percentage of average pixel error compared to image width and height are 2.48% and 3.30%, respectively. Similarly, the percentage of maximum error compared to the image width and height are 11.47% and 15.27%. From these results, it is possible to conclude that even when pixels are saturated, event-based docking port detection works. Conventional cameras are not expected to operate in these high-illuminated and saturated conditions.

V. CONCLUSIONS

RGB cameras suffer from key shortcomings in satellite docking applications, mainly owing to extreme illumination conditions. This paper presents a LEO simulation environment setup for satellite docking experiments using event cameras. By using event cameras and the proposed pipeline in this paper, we demonstrate that it is possible to produce consistent detection of navigational aids under adverse illumination conditions. The proposed pipeline can be used to determine the preliminary orientation information of a standard docking port. Future work will involve temporal consistency of detection, 6 DoF pose estimation and tracking.

REFERENCES

[1] P. Lichtsteiner, C. Posch, and T. Delbruck, "A 128× 128 120 db 15 μs latency asynchronous temporal contrast vision sensor," *IEEE Journal of Solid-State Circuits*, vol. 43, no. 2, pp. 566–576, 2008.

[2] Lockheed Martin, "Lockheed Martin Mission Augmentation Port (MAP) Standard," Lockheed Martin, Tech. Rep., 2022.

[3] S. Afshar, A. P. Nicholson, A. van Schaik, and G. Cohen, "Event-Based Object Detection and Tracking for Space Situational Awareness," *IEEE Sensors Journal*, vol. 20, no. 24, pp. 15 117–15 132, 12 2020.

[4] G. Gallego, T. Delbruck, G. Orchard, C. Bartolozzi, B. Taba, A. Censi, S. Leutenegger, A. J. Davison, J. Conradt, K. Daniilidis, and D. Scaramuzza, "Event-Based Vision: A Survey," *IEEE Transactions on Pattern Analysis and Machine Intelligence*, vol. 44, no. 1, pp. 154–180, 1 2022.

[5] A. Glover and C. Bartolozzi, "Event-driven ball detection and gaze fixation in clutter," in *2016 IEEE/RSJ International Conference on Intelligent Robots and Systems (IROS)*. IEEE, 10 2016, pp. 2203–2208.

[6] A. Amir, B. Taba, D. Berg, T. Melano, J. McKinstry, C. Di Nolfo, T. Nayak, A. Andreopoulos, G. Garreau, M. Mendoza, J. Kusnitz, M. Debole, S. Esser, T. Delbruck, M. Flickner, and D. Modha, "A Low Power, Fully Event-Based Gesture Recognition System," in *2017 IEEE Conference on Computer Vision and Pattern Recognition (CVPR)*. IEEE, 7 2017, pp. 7388–7397.

[7] H. Rebecq, G. Gallego, E. Mueggler, and D. Scaramuzza, "EMVS: Event-Based Multi-View Stereo—3D Reconstruction with an Event Camera in Real-Time," *International Journal of Computer Vision*, vol. 126, no. 12, pp. 1394–1414, 12 2018.

[8] A. R. Vidal, H. Rebecq, T. Horstschaefer, and D. Scaramuzza, "Ultimate SLAM? Combining Events, Images, and IMU for Robust Visual SLAM in HDR and High-Speed Scenarios," *IEEE Robotics and Automation Letters*, vol. 3, no. 2, pp. 994–1001, 4 2018.

[9] R. Benosman, C. Clercq, X. Lagorce, Sio-Hoi Ieng, and C. Bartolozzi, "Event-Based Visual Flow," *IEEE Transactions on Neural Networks and Learning Systems*, vol. 25, no. 2, pp. 407–417, 2 2014.

[10] S. Bagchi and T.-J. Chin, "Event-based Star Tracking via Multiresolution Progressive Hough Transforms," in *2020 IEEE Winter Conference on Applications of Computer Vision (WACV)*. IEEE, 3 2020, pp. 2132–2141.

[11] G. Cohen, S. Afshar, B. Morreale, T. Bessell, A. Wabnitz, M. Rutten, and A. van Schaik, "Event-based Sensing for Space Situational Awareness," *The Journal of the Astronautical Sciences*, vol. 66, no. 2, pp. 125–141, 6 2019.

[12] M. Jawaid, E. Elms, Y. Latif, and T.-J. Chin, "Towards Bridging the Space Domain Gap for Satellite Pose Estimation using Event Sensing," in *2023 IEEE International Conference on Robotics and Automation (ICRA)*. IEEE, 5 2023, pp. 11 866–11 873.

[13] N. W. Oumer, G. Panin, Q. Mülbauer, and A. Tseneklidou, "Vision-based localization for on-orbit servicing of a partially cooperative satellite," *Acta Astronautica*, vol. 117, pp. 19–37, 12 2015.

[14] S. Ruel, T. Luu, and A. Berube, "On-orbit testing of target-less TriDAR 3D rendezvous and docking sensor," in *Proc of the International Symposium on Artificial Intelligent, Robotics and Automation in Space (i-SAIRAS 2010)*, 2010.

[15] C. Samson, C. English, A. Deslauriers, I. Christie, F. Blais, and F. Ferrie, "Neptec 3D laser camera system: From space mission STS-105 to terrestrial applications," *Canadian Aeronautics and Space Journal*, vol. 50, no. 2, pp. 115–123, 2004.

[16] iniVation, "DAVIS 346," 2019. [Online]. Available: https://inivation.com/wp-content/uploads/2019/08/DAVIS346.pdf

[17] A. Yol, E. Marchand, F. Chaumette, K. Kanani, and T. Chabot, "Vision-based navigation in low earth orbit," in *Int. Symp. on Artificial Intelligence, Robotics and Automation in Space, i-SAIRAS'16*, Beijing, 6 2016.

[18] Kaichao You, "Event Camera: the Next Generation of Visual Perception System." [Online]. Available: https://spectra.mathpix.com/article/2022.03.00339/event-camera-the-next-generation-of-visual-perception-system

[19] O. Ronneberger, P. Fischer, and T. Brox, "U-Net: Convolutional Networks for Biomedical Image Segmentation," 2015, pp. 234–241.

[20] T. Y. Zhang and C. Y. Suen, "A fast parallel algorithm for thinning digital patterns," *Commun. ACM*, vol. 27, no. 3, p. 236–239, mar 1984. [Online]. Available: https://doi.org/10.1145/357994.358023